A Study on Drum Cutting Properties with Full-scale Experiments and Numerical Simulations

Xuefeng Li [1], Shibo Wang [1, 2,*], Shirong Ge [1, 2], Reza Malekian [3], Zhixiong Li [1, 4], Yifei Li[5]

[1] School of Mechanical Engineering, China University of Mining and Technology, Xuzhou 221000, China; leexf2009@163.com (X.L.); wangshb@cumt.edu.cn (S.W.); gesr@cumt.edu.cn (S.G.); zhixiong.li@ieee.org (Z.L.)

[2] Collaborative Innovation Center of Intelligent Mining Equipment, China University of Mining and Technology, Xuzhou 221000, China;

[3] Department of Electrical, Electronic & Computer Engineering, University of Pretoria, Pretoria 0002, South Africa; reza.malekian@ieee.org (R.M.)

[4] School of Mechanical and Manufacturing Engineering, University of New South Wales, Sydney 2052, Australia

[5] Department of Mechanical Engineering, Iowa State University, Ames, IA, 50011, USA; yifei.li@iastate.edu (Y.L.)

***** Correspondence: wangshb@cumt.edu.cn; Tel.: +86-516-8359-0709; Fax: +86-516-8359-1916

Abstract: In order to investigate the properties of cutting loads on shearer drum, a series of full-scale shearer drum cutting tests were conducted in the National Energy Coal Mining Machinery Equipment Research and Design Center of China. The pick forces and the torque acting on the drum were measured and recorded under different cutting conditions by the strain sensors that were embedded in the cutting picks. Besides, an attempt was made to simulate the shearer drum cutting process. For this purpose, a computer program named Particle Flow Code in three dimensions (PFC3D) based on discrete element method (DEM) was used. The rock sample was models by graded particle assemblies and the micro-properties were calibrated by modeling the uniaxial compressive strength tests. The cutting process for the front and back drums with different traction speeds were simulated with this model. The torque of drums and forces of each pick were obtained during the simulation. Reasonable agreement and significant correlations were found between experiment and numerical simulation in terms of cutting forces of picks and the mean torque of the drums. The specific energy increased with the increase of traction speed in experiments, which was reproduced well in numerical simulation. Moreover, according to the analysis in frequency domain, the vibration of drum torque consists of components with multiple frequencies below 50 Hz, which is observed in both experiment and simulation. Therefore, numerical simulation by PFC3D is an easier, faster and reasonable method in the prediction of drum cutting load and design of shearer drum.

Keywords: drum cutting; full-scale experiment; particle flow code; numerical simulation

1. Introduction

Although the technologies of new energies (like solar energy, wind energy, nuclear energy and biomass energy, etc.) develop very fast currently, the fossil energy is still the main energy source across the world. In China, the proportion of fossil energy in the total energy consumed is still approximately 87% and the proportion of coal is about 63% in 2016 reported by the National Energy Administration [1]. Long-wall mining with a shearer is the mostly used method in underground coal mining. The production and productivity of long-wall mining depend on the cutting properties of the shearer for a long-wall working face. Meanwhile, the cutting load, as the working load of a shearer, is the criterion in designing the shearer. So the design and cutting properties evaluation of the shearer drums are very important for improving not only the productivity of long-wall face but also the reliability of the shearer.

In order to understand the cutting properties of the drum, researchers have carried out substantial theoretical, experimental and simulation work on shearer drum cutting load prediction. E.3. et al. [2] proposed a theoretical model in prediction shearer drum cutting load by the mean cutting force of picks based on experiments considering the effects of rock property, pick geometry and working condition of the shearer. Liu

et al. [3] improved the model established in reference [2] by importing gangues randomly considering the anisotropy of the coal seam. Hekimoglu [4] investigated the cutting loads of picks on a shearer drum in laboratory, and found that the plate picks were subjected to the higher forces than those on vanes. Khair [5] built the automated rotary cutting simulator (ARCCS) shown in Figure 1(a). With ARCCS, the effects of pick geometry, pick line space, cutting depth, dip angle of picks and rotation speed on the particle distribution and cutting load were studied [6,7]. Addala [8] and Qayyum [9] investigated the effect of tip angle of picks on the cutting load and specific energy in drum cutting with ARCCS. Liu et al. [10] built the rotary cutting tester (Figure 1(b)) and conducted drum cutting tests with five types of picks with different geometries and ten drums with different pick arrangements. They found the relationship between cutting performance parameters (i.e. drum cutting load, specific energy and lump coal rate) and the parameters of the drum structure and kinematics. However, the drums used in these cutting testers are shrunken and simplified, viz., small-scale testers. Small-scale tests are meaningful for the design of drum structure, but the cutting loads obtained from small-scale tests are difficult to be directly used in shearer design considering the difference in terms of scale, boundary condition and working condition from the real shearer drum. In addition, Camargo et al. [11] reported a type of instrumented bit developed by National Institute for occupational safety and health. The instrumented bit is self-contained, intrinsically safe and capable of measuring coal cutting forces in three orthogonal directions. In-situ experiments with this instrumented bit were conducted in three mines to obtain the coal cutting forces. Eyyuboglu and Bolukbasi [12] investigated the effects of equal and unequal circumferential pick spacing on the performance of road-headers by conducting in-situ experiments in Park Cayirhan Coal Mine in Turkey. Through in-situ experiment is the most reliable method to obtain the cutting forces, it is costly and difficult, and there is no appropriate opportunity to conduct in-situ experiments in mines for most researchers. Moreover, full-scale cutting tests were conducted in laboratory with a real shear drum and large rock samples in order to eliminate the influence of scale and boundary condition on the results. Hekimoglu and Ozdemir [13] carried out a series of full-scale cutting tests with a two-start drum in the Earth Mechanics Institute at Colorado School of Mines to investigate the effect of wrap angle on cutting load of the drum.

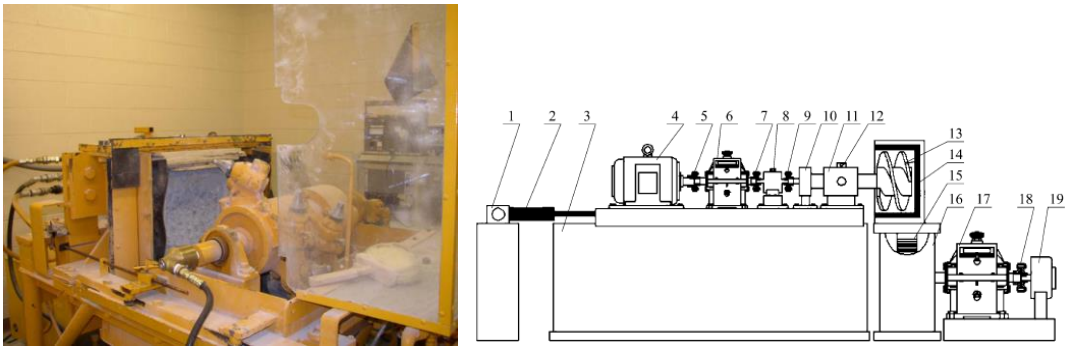

(a) (b)

Figure 1. The automated rotary cutting simulator in West Virginia University (a) and rotary cutting tester in China University of Mining and Technology (b)

As an easier and faster method, the numerical simulation is widely used in the prediction of tool forces. Yu [14] and Mishra [15] built the rotary drum cutting model with LS-DYNA and ABAQUS/Explicit based on the finite element method (FEM), respectively, to investigate the effects of rotation speed and pick geometry on the drum cutting loads. However, the FEM is disabled in modeling the discontinuities and anisotropy of coal. Particle Flow Code in three dimensions (PFC3D) based on discrete element method (DEM) is widely used in simulating the rock cutting process in engineering filed since it models rocks as an assembly of particles with discontinuities and cracks. Although many attempts have been made to simulate the rock cutting process with a pick by PFC3D and matched well with experiments [16-18], very limited work has been done to address the drum cutting process simulation using PFC3D. Moreover, to the best of our knowledge, the verification of the PFC3D-based coal cutting force model using full-scale drum cutting tests

has not been found yet. It is important to use experimental data acquired from the full-scale drum cutting tests to verify the correctness and reliability of the PFC3D model.

In order to address the aforementioned issue, this paper models the drum cutting process under different cutting conditions with PFC3D and compares the results with those obtained from full-scale drum cutting tests. A series of full-scale shearer drum cutting tests were conducted with different traction speeds, and the cutting forces of picks and the torque of the drum were obtained using strain sensors embedded in the cutting picks. The relationships between the simulation and experiments results (i.e. pick cutting forces, drum torque and specific energy) were discussed using regression analysis and frequency analysis.

The rest of this paper is organized as follows. Section 2 presents a series of full-scale shearer drum cutting tests. The PFC3D-based coal cutting force model is designed in Section 3, and Section 4 performs the validation and discussion on the cutting force analysis results obtained from the experiments and simulations. The paper is concluded in Section 5.

2. Experimental studies

2.1. Full-scale shearer cutting test

The full-scale shearer cutting tests were conducted in the National Energy Coal Mining Machinery Equipment Research and Design Center of China. A full-scale mechanized mining face was built in this laboratory with a real shearer, scrapper and hydraulic supporters, as shown in Figure 2. The parameters of the shearer are listed in Table 1. A series of shearer cutting tests were conducted with traction speeds of 1.5, 3 and 5 m/min and rotation speed of 28 rpm. The mining height and mining depth are 2700 mm and 500 mm in the experiments, respectively. The tangential force (F_t) of an idler shaft in the ranging arm gearbox was measured with a force sensor, as shown in Figure 3. The torque acting on the idler shaft was calculated with Eq. (1)

$$T = \frac{F_{t1} \cdot d}{2} = \frac{F_t \cdot d}{4} \tag{1}$$

where T is the torque acting on the idler shaft, d is the diameter of the idler, F_{t1} is the tangential force acting on the idler. The torque acting on the drum was calculated based on the torque acting on the idler shaft and the transmission ratio between the idler and the drum as shown in Eq. (2)

$$M = r \cdot T = \frac{r \cdot F_t \cdot d}{4} \tag{2}$$

where M is the torque acting on the shearer drum, r is the transmission ratio between the idler and the drum.

Table 1. Parameters of the MG500/1130 shearer

Parameter	Value	Parameter	Value
Drum diameter	Φ1800 mm	Drum rotation speed	28 r/min
Installed pawer	2×500+2×55+20 kW	Traction speed	0~13.8 m/min
Mining height	1800~3760 mm	Traction force	680~410 kN
Mining depth	0~800 mm	\	\

The pick forces were measured during the shearer cutting process with strain sensors fixed on some selected picks, i.e. measurement picks, as shown in Figure 4. The signal of pick cutting force was transferred to the monitoring center by wireless transmission modules. The forces acting on the pick consist of three orthogonal forces in a local coordinate system shown in Figure 4(b). *Fx* is the force perpendicular to the axis of the pick, *Fy* is the sideway force, *Fz* is the force along the axis of the pick.

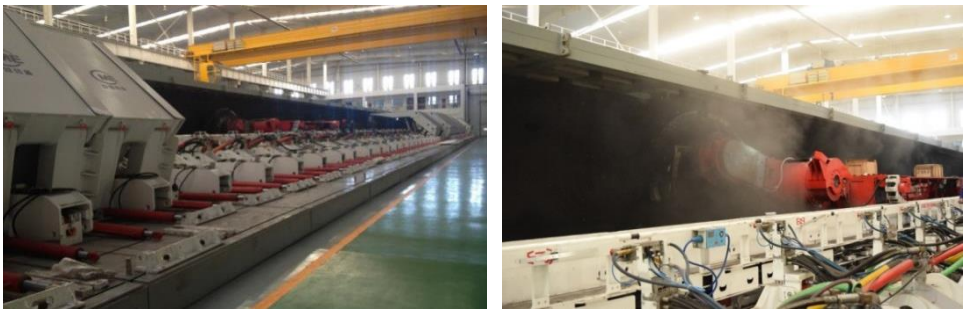

Figure 2. Simulative full-scale mechanized mining face in National Energy Coal Mining Machinery Equipment R & D Center

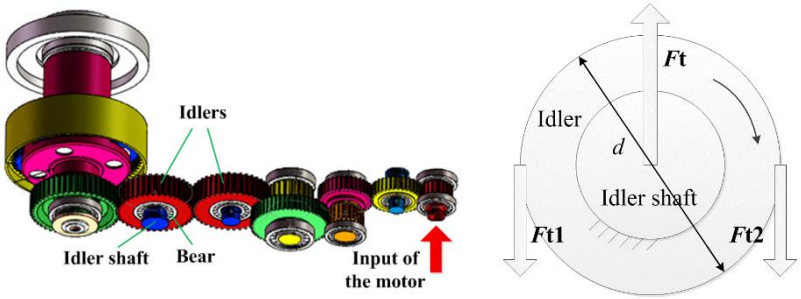

(a) (b)

Figure 3. Schematic of (a) mechanical drive of shearer ranging arm and (b) forces acting on idler shaft

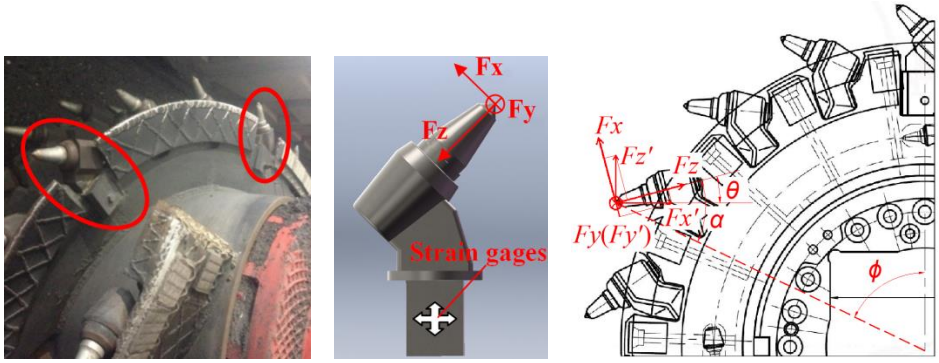

(a) (b) (c)

Figure 4. The photo (a) and schematic (b) of the measurement picks and schematic of cutting forces acting on a pick (c)

2.2. Rock mechanical properties test

In order to build the artificial coal mass model in PFC3D, the uniaxial compressive strength (UCS) and Brazilian tensile strength (BTS) of artificial coal samples were measured according to ASTM standards (American Society of Testing Materials D2938 and D3967) [19,20], as shown in Figure 5. Each test was repeated at least three times. The properties of the artificial coal mass are UCS of 12.25 MPa, Young's modulus of 0.319 GPa, Poisson's ratio of 0.331 and BTS of 1.19 MPa.

(a) (b) (c)

Figure 5. Photos of (a) rock property test equipment and fracture patterns in (b) UCS test and (c) BTS test

2.3. Experimental results

Figure 6 shows the variation of pick forces in the local coordinate system during one cutting cycle with the traction speed of 1.5 m/min. The variation of the forces of *Fx* and *Fz* firstly increased with fluctuation due to rock chip formation, and then decreased to zero, which is in accord with the variation of the cutting depth of the pick (shown in Figure 7) in one cutting period. The lateral force of *Fy* fluctuates around zero.

Figure 8 shows the measurements of the torque acting on the front and back drums with different traction speeds. It is noted that both the mean value and standard deviation of the torque increase linearly with the increase of traction speed. As shown in Figure 9, there are strong linear relationships with the correlation coefficient of at least 0.9394 between the mean value and standard deviation of the torque and traction speed. With the increase of the traction speed, the cutting area of the drum in each cutting period increased. The larger cutting area resulted in forming larger chips. Consequently, the mean value and standard deviation of the torque increase with the increase of traction speed.

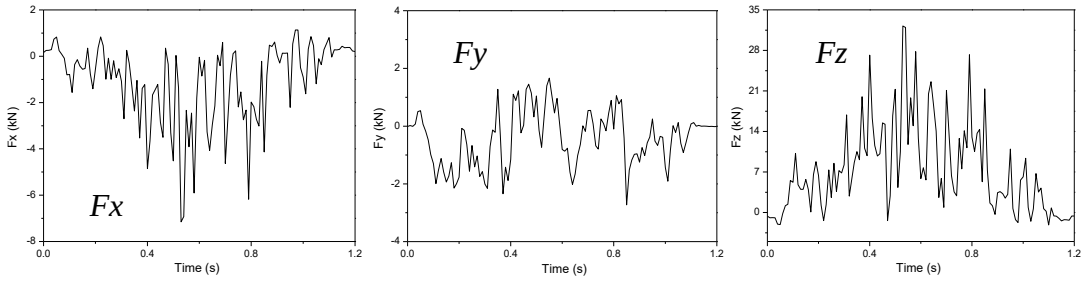

Figure 6. Measurements of forces in three dimensions acting on the pick in one cutting period

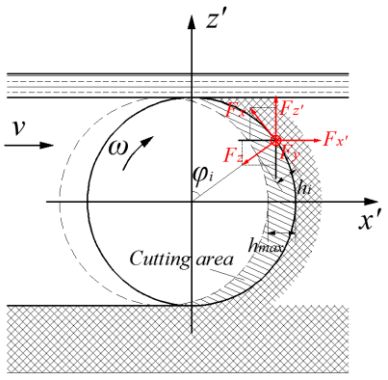

Figure 7. Schematic of the shearer drum cutting process

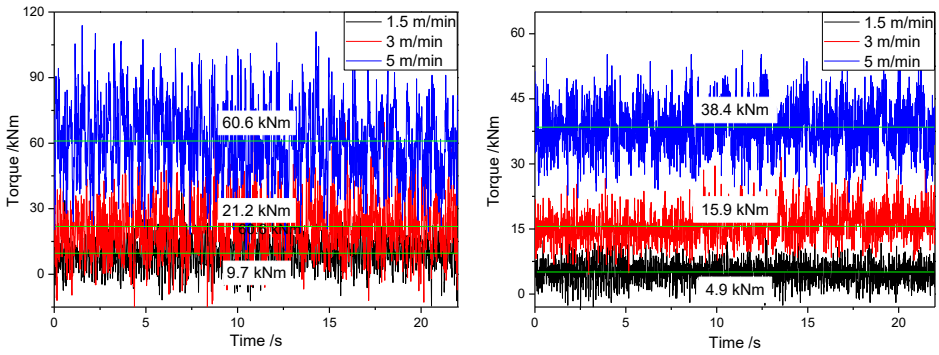

(a) (b)

Figure 8. Measurements of the torque acting on the drum with different traction speeds: (a) the front drum and (b) the back drum

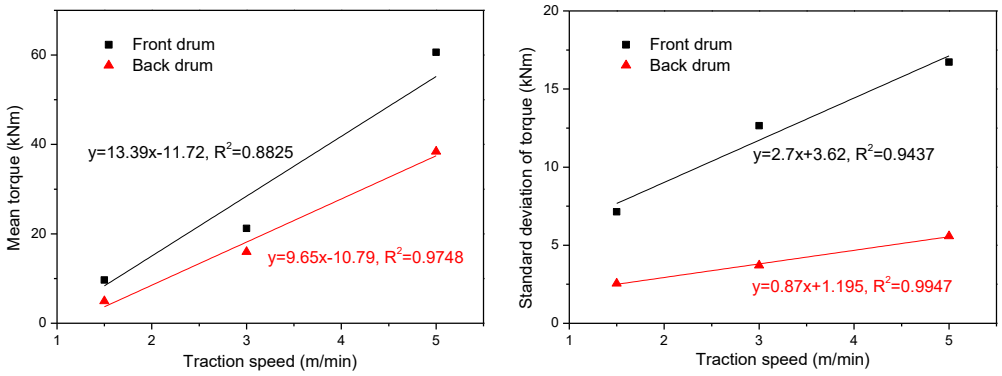

(a) (b)

Figure 9. Relationships between mean value and standard deviation of the torque acting on drums and traction speed

3. Numerical simulative studies

3.1. Model of Shearer drum cutting test

Figure 10 shows the shearer drum cutting model for the front and back drums. In order to improve the efficiency of simulation, the model of coal mass is graded by particle radius [21]. Firstly, a cubic particle assemble with particle radii of 20 to 50 mm was generated and calculated to a stable stage, namely layer 2 shown in Figure 10(a). Then, the particles in the cutting region were deleted and filled with small particles (layer 1) with radii of 5~20 mm. The coal mass sample was generated as large as possible to minimize the boundary effects and obtain the similar cutting condition to that in the laboratory. The dimensions of the coal mass are 3.6, 2.16 and 4.32 m in length, width and height, respectively. Particles in a half cylinder region with a diameter of 1.8 m were deleted for arranging the shearer drum for the front drum cutting model. The right and front walls of the coal specimen were deleted. The drum model of MG500/1130 shearer was built using 3D design software of Solidworks and imported into PFC3D. The shearer drum is an assembly including picks, spiral vanes and drum hub. Each part of the drum is a separate wall regarded as a rigid body. Consequently, the cutting loads of each pick can be recorded. Different with the front drum cutting model, the particles in the region above the center of the drum were deleted in the back drum cutting model shown in Figure 10(b) for the mining height of the back drum was 0.9 m in the experiment. There are approximately 0.344 million particles for the front drum cutting model and 0.215 million particles for the back drum cutting model.

The parallel bond contact model was used in building the coal sample in PFC3D. The micro parameters of parallel bond for the artificial coal sample were calibrated by modeling UCS tests [22] for particle

assembles with different radii, which are listed in Table 2. The macro properties of the coal sample in laboratory and simulation are summarized in Table 3.

During the cutting simulation process, the forces acting on the pick were monitored [23-24]. The directions of pick forces obtained from simulation and tests are different, as shown in Figure 4(c). For comparison, the forces recorded in PFC3D were transformed from the global to local coordinate system by Eq. (3)

$$\begin{cases} Fx = -Fx' \cdot \sin\theta + Fz' \cdot \cos\theta \\ Fy = Fy' \\ Fz = -Fx' \cdot \cos\theta - Fz' \cdot \sin\theta \\ \theta = \pi/2 - \alpha - \phi \end{cases} \tag{3}$$

where *Fx'*, *Fy'* and *Fz'* are the forces acting on the pick in the global coordinate system, θ is the angle between the global and local coordinate systems, α is the angle between the axis of the pick and the linear connecting the tip of the pick and the center of the drum, ϕ is the rotation angle of the pick.

The torque acting on the drum was calculated in PFC3D with FISH (a kind of programming language embedded in PFC3D) by Eq. (4).

$$\begin{cases} M_i = Fx' \cdot D\cos\phi/2 + Fz' \cdot D\sin\phi/2 \\ M = \sum_{i=1}^{N} M_i \end{cases} \tag{4}$$

where M_i is the moment of the *i*th pick about the drum center, *M* is the torque acting on the drum, *N* is the number of picks.

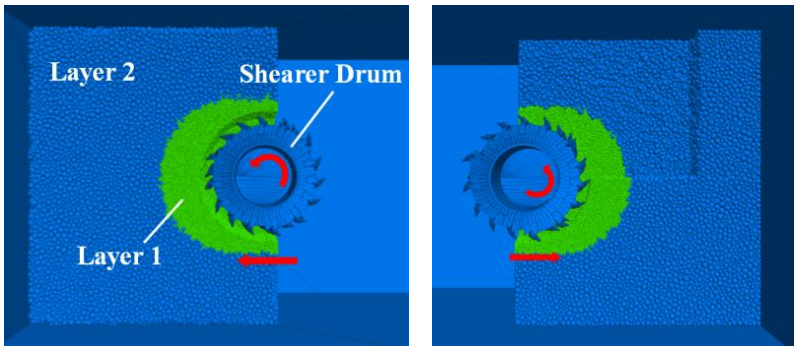

(a) (b)

Figure 10. Shearer drum cutting models: (a) the front drum and (b) the back drum

Table 2. Micro parameters of coal model

Micro parameters	Layer 1	Layer 2
Particle radius (*r*, mm)	5-20	20-50
Bond elastic modulus (GPa)	0.14	0.16
Bond stiffness ratio (*kn*/*ks*)	2.8	2.8
Bond tensile strength (MPa)	3.3±1	12.5±1
Bond shear strength (MPa)	30±1	37.5±1
Particle elastic modulus (*E'*, GPa)	0.14	0.16
Particle stiffness ratio (*k'n*/*k's*)	2.8	2.8

Table 3. Macro properties of coal specimen

Property	Laboratory test	Simulation	
		Layer 1	Layer 2
UCS (MPa)	12.25	13.13	13.69
E (GPa)	0.319	0.295	0.303
μ	0.23	0.228	0.228

3.2. Simulation results of front drum

In consistent with the experiment mentioned above, the simulation of front drum cutting process were conducted with drum rotation speed of 28 r/min and traction speed of 1.5 m/min, 3 m/min and 5 m/min. Figure 11 shows the variation of experimental and simulative pick forces of the front drum in one cutting period. It was noted that the forces obtained in simulation matched well with the experimental results in magnitude and fluctuation tendency. Figure 12(a)-(c) shows the vibration of torque acting on the front drum with different traction speeds. In different cutting conditions, there is an increase stage of the torque responding to the process that the drum cut into the coal mass. A stable stage of the torque is observed when the displacement of the drum is about 0.075 m. The mean value and standard deviation of the torque in the stable stage were calculated, as shown in Figure 12(d). Both the mean value and standard deviation increase linearly against the traction speed with a high correlation coefficient of at least 0.9967.

Figure 13 shows the fragment pattern in the drum cutting process with different traction speeds. In these figures, the chips were cut and transported mostly to the goaf reflecting the loading efficiency of the drum in a certain cutting condition to some extent, which is a significant factor in designing drums by this model in our further study.

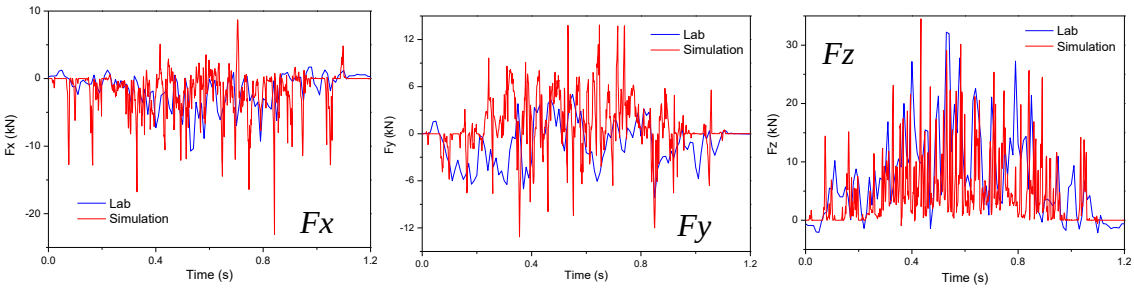

Figure 11. Comparison between experimental and simulative vibrations of forces in three dimensions acting on a pick of the front drum in one cutting period

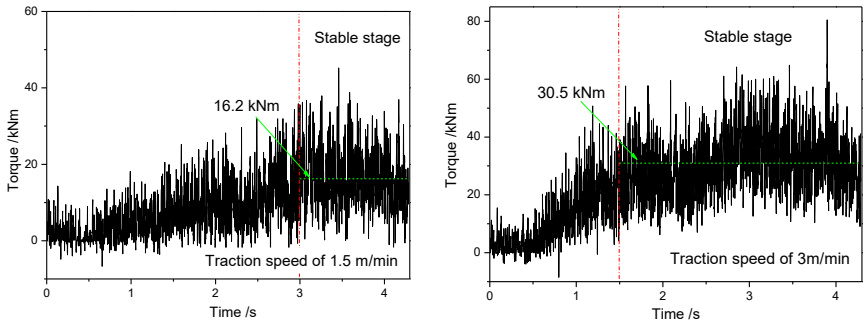

(a) (b)

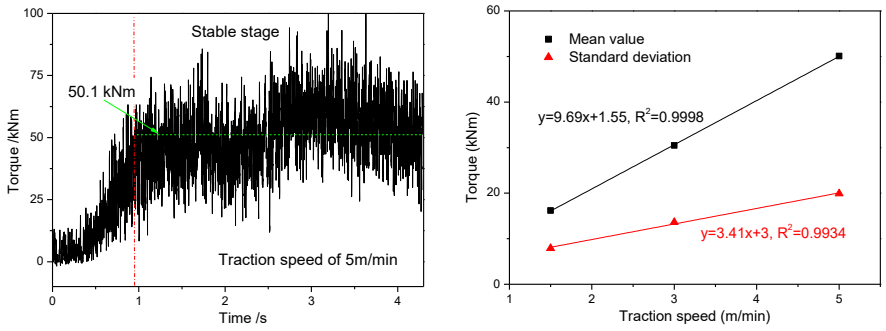

(c) (d)

Figure 12. Vibrations of the torque acting on the front drum with different traction speeds (a-c) and relationship between traction speed and the torque acting on the drum (d)

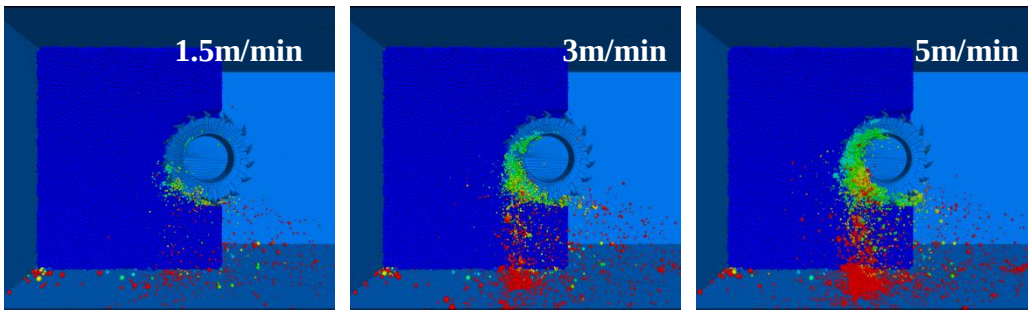

Figure 13. Fragment patterns in front drum cutting simulation with different traction speeds

3.3. Simulative results of back drum

Figure 14 shows the cutting process of the back drum with traction speed of 5 m/min. Due to the existence of the free surface, larger chips were formed periodically compared with the front drum cutting simulation. Figure 15 shows the pick forces comparison between experiment and simulation of the back drum in one cutting period. It was indicated that the forces obtained in simulation matched well with the experimental results. Figure 16(a)-(c) shows the vibration of torque acting on the back drum with different traction speeds. A stable stage of the torque is also observed when the displacement of the drum is about 0.075 m. The mean value and standard deviation of the torque in the stable stage were calculated shown in Figure 16(d). Both the mean value and standard deviation increase linearly with the increase of traction speed with a high correlation coefficient of at least 0.9993.

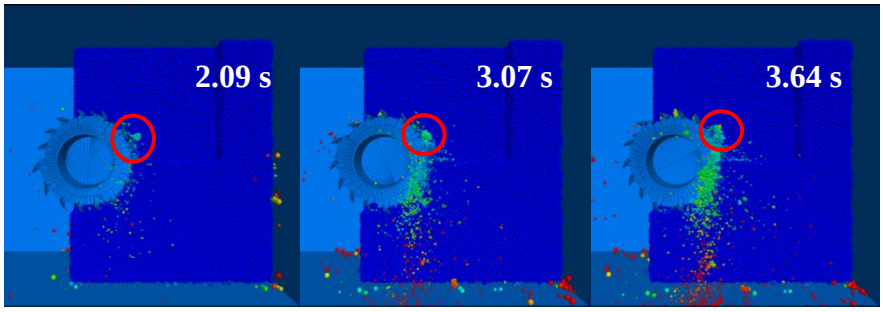

Figure 14. Cutting process of the back drum with the traction speed of 5m/min

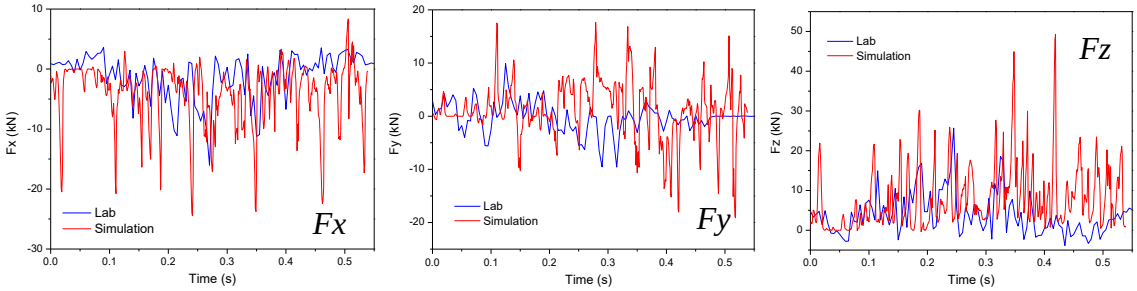

Figure 15. Comparison between experimental and simulative vibrations of forces in three dimensions acting on a pick of the back drum in one cutting period

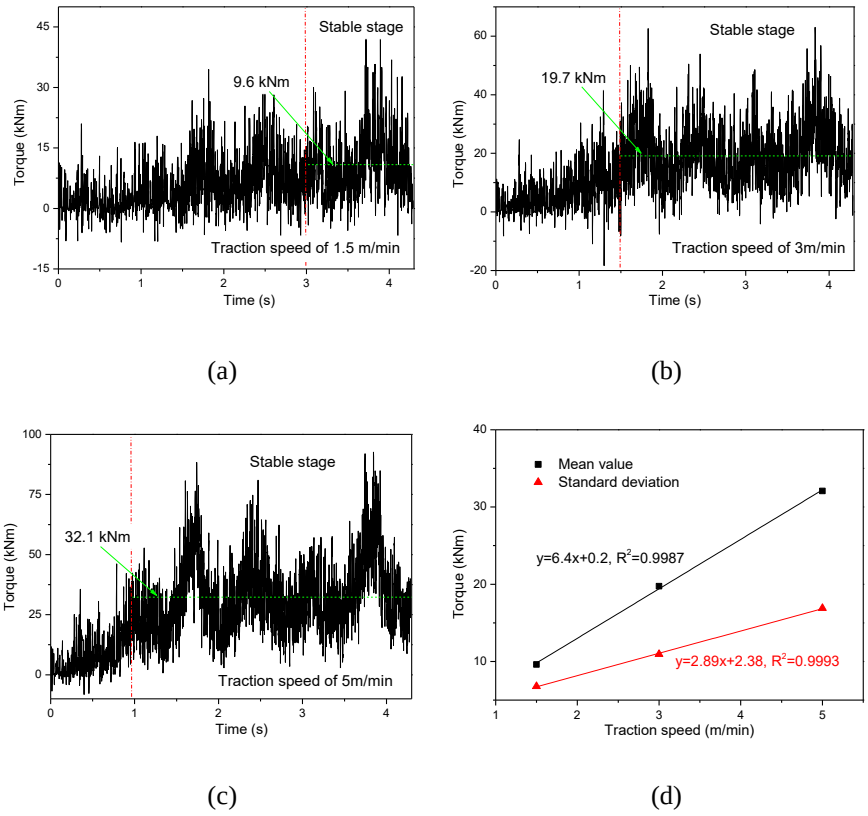

Figure 16. Vibration of torque acting on the back drum with different traction speed (a-c) and relationship between traction speed and the torque acting on the drum (d)

4. Validation and discussion

In order to evaluate the fluctuation of the drum torque, the fluctuation coefficients of drum torque obtained from experiment and simulation were calculated by Eq. (5) [25].

$$k = \frac{1}{\bar{M}} \cdot \frac{1}{n} \sum_{i=1}^{n} \left| M_i - \bar{M} \right| \tag{5}$$

where k is the fluctuation coefficient, $\bar{M}$ is the mean drum torque (kNm), M_i is the ith value of drum torque, n is the number of data. The fluctuation coefficient indicates the relative fluctuation amplitude of drum torque [26]. The larger k is, the more violently the drum torque fluctuates. For the purpose of evaluating the cutting efficiency of the drum in different conditions, the specific energy (SE) [27, 28] in experiment and simulation was calculated by Eq. (6).

$$SE = \frac{\bar{M} \cdot \omega \cdot t}{V}, \text{where } V = \begin{cases} vt \cdot l \cdot H, Experiment \\ \frac{1}{p}\sum_{i=1}^{N} V_i, Simulation \end{cases} \quad (6)$$

where $\bar{M}$ is the mean torque acting on the drum, ω is the angular velocity of the drum, t is the cutting time, V is the volume of coal mass cut, v is the traction speed of the shearer, l is the mining depth of the drum, H is the mining height, p is the porosity of coal sample in PFC3D, N is the total number of the spalled particles, V_i is the volume of the ith particle.

The results of mean torque, fluctuation coefficient and SE obtained from experiment and simulation are summarized in Table 4. The results in terms of drum torque of simulation are larger than those of experiment with the traction speeds of 1.5 m/min and 3 m/min while it's adverse in the condition of 5 m/min. The similar laws were found in terms of SE. The reason for the difference between experiment and simulation is probably due to the effect of rock anisotropy. The coal model in simulation is consisted of discontinuous particles with the same micro parameters in the cutting region while the artificial coal mass in experiment is a mixture of cement, coal, rock, etc. The cutting depth of picks increases with the increase of traction speed, which decreases the influence of rock anisotropy. The results of simulation matched better with those of experiment in the condition of larger traction speed. Figure 17 depicts the relationships between mean torques obtained from experiment and simulation. Significant linear correlations were found between them with a correlation coefficient of at least 0.9534. Figure 18 manifests the relationships between traction speed and fluctuation coefficient. As shown in Figure 18, the torque fluctuation coefficient decreases with the increase of traction speed. It notes that the relative fluctuation amplitude decreases with the increase of traction speed. Although the standard deviation of torque increases with the increase of traction speed mentioned above, the torque fluctuates more stable in the condition of high traction speed. Besides, the torque fluctuation coefficients of back drum are larger than those of front drum for both experiment and simulation. This is because the up free surface in the cutting process of back drum results in large chip formation which is observed in the back drum cutting simulation. Consequently, the shearer drum cutting model built by PFC3D is reasonable and reliable in the prediction of the loads acting on the drum in different cutting conditions.

Figure 19 describes the relationship between traction speed and specific energy obtained from experiment and numerical simulation. SE increases with the increase of traction speed in the investigated spectrum in both experiment and numerical simulation. The increment of spalled coal volume is less than the increment of the drum torque with the increase of traction speed. When the traction speed is small in numerical simulation, the short stable stage results in that the statistical chip volume in PFC3D is smaller than the theoretical value, which is the reason for the difference between numerical simulation and experiment in terms of SE. Consequently, it will be better if the simulation were conducted for more time in the condition of low traction speed. Even so, the numerical simulation is reasonable in reproducing the relationship between traction speed and energy consumption comparing with experiment.

Table 4. Results of mean torque, fluctuation coefficient and specific energy obtained from experiment and simulation

Traction Speed	Experiment						Simulation					
m/min	$\bar{M}_{ef}$	k_{ef}	SE_{ef}	$\bar{M}_{eb}$	k_{eb}	SE_{eb}	$\bar{M}_{sf}$	k_{sf}	SE_{sf}	$\bar{M}_{sb}$	k_{sb}	SE_{sb}
1.5	9.67	0.406	1259.3	4.94	0.582	1287	16.19	0.377	1600.3	9.62	0.581	2081.4
3	21.2	0.184	1380.7	15.96	0.473	2078.3	30.46	0.265	2105	19.74	0.4	2992.5
5	60.62	0.116	2368.2	38.41	0.221	3001.1	50.09	0.215	2137	32.07	0.364	2883.7

where the subscripts of *ef* and *eb* represent the results of the front and back drums, respectively, obtained from experiment, the subscripts of *sf* and *sb* represent the results of the front and back drums, respectively, obtained from simulation, the units of M and SE are kNm and kW/m^3, respectively.

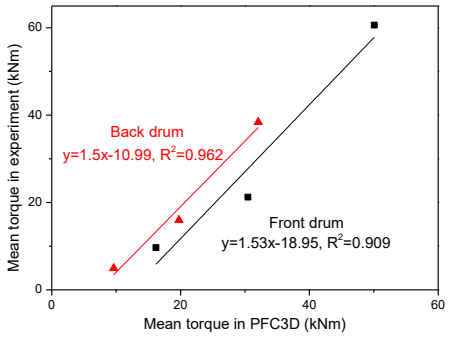

Figure 17. Relationship between mean torques obtained from experiment and simulation

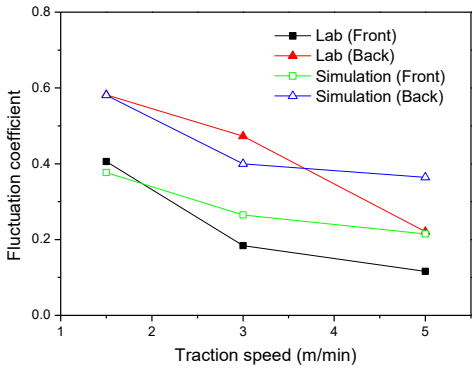

Figure 18. Relationship between traction speed and fluctuation coefficient

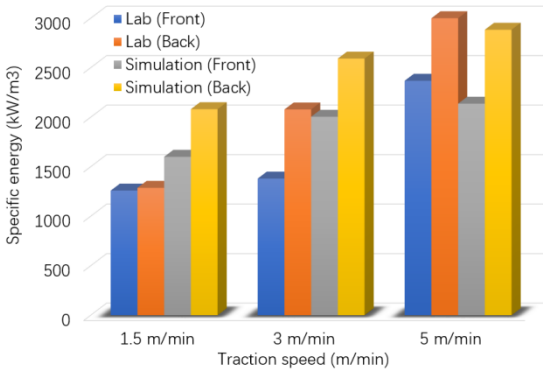

Figure 19. Relationship between traction speed and specific energy

Drum torque fluctuation is correlated with chip formation process. For more details of torque fluctuation, analysis of drum torque in frequency domain was carried out by empirical mode decomposition (EMD) [29] method and power spectral density (PSD) analysis [30]. EMD is pioneered by Huang et al. for adaptively representing nonstationary signals as sums of intrinsic mode functions (IMF) in time domain ordered by frequency [31]. Each IMF is a separate signal [32,33]. Consequently, more details can be obtained by analysis of IMFs in frequency domain by PSD analysis. Firstly, the original torque signals were decomposed into 10 IMF components and one residual component in each case with EMD method. Figure 20 shows the EMD results of the torque of front-drum with traction speed of 1.5 m/min in experiment and simulation. The 10 IMF components in each case are ordered by frequency from IMF1 to IMF10. And then, the analysis of IMF1~IMF8 in frequency domain by PSD analysis were conducted as shown in Figure 21. As the sampling frequency is 100 Hz in experiment, the frequency range is 0~50 Hz in the analysis of experimental torque in frequency domain. The analysis of simulative torque ranges from 0 to 500 Hz since the sampling frequency is 1000 Hz in simulation. As shown in Figure 21, there is a characteristic frequency for each IMF component of experimental torque. However, for the IMF components with high frequency (i.e.

IMF1, IMF2) of simulative torque, the curve of PSD is almost continuous with smaller amplitudes comparing to low frequency components. For the IMF components with low frequency of simulative torque, discrete characteristic frequencies were similar to the experimental results. The characteristic frequencies of front-drum torque under different cutting conditions in experiment and simulation are summarized in Table 5. Take the PSD analysis result in the condition of 1.5 m/min of traction speed as an example, the characteristic frequency of IMF7 (0.4639 Hz) of experimental torque is the base frequency since the rotate speed of the drum is 28 rpm, i.e. 0.4667 Hz. The second, third, seventh, fifteenth harmonics of the base frequency were respectively observed at the characteristic frequencies of IMF6, IMF5, IMF4 and IMF3. This is because of the formation of rock chips with different particle size during cutting. The similar characteristic frequencies were obtained from the PSD analysis of simulative torque signal for the low frequency components (< 50 Hz). Besides, the amplitudes at the high characteristic frequency (>50 Hz) are much smaller than those at low frequency. This suggests that the vibration of the torque is composed of components with multiple frequencies below 50 Hz. Consequently, the drum torque is reproduced well by the PFC3D model in frequency domain.

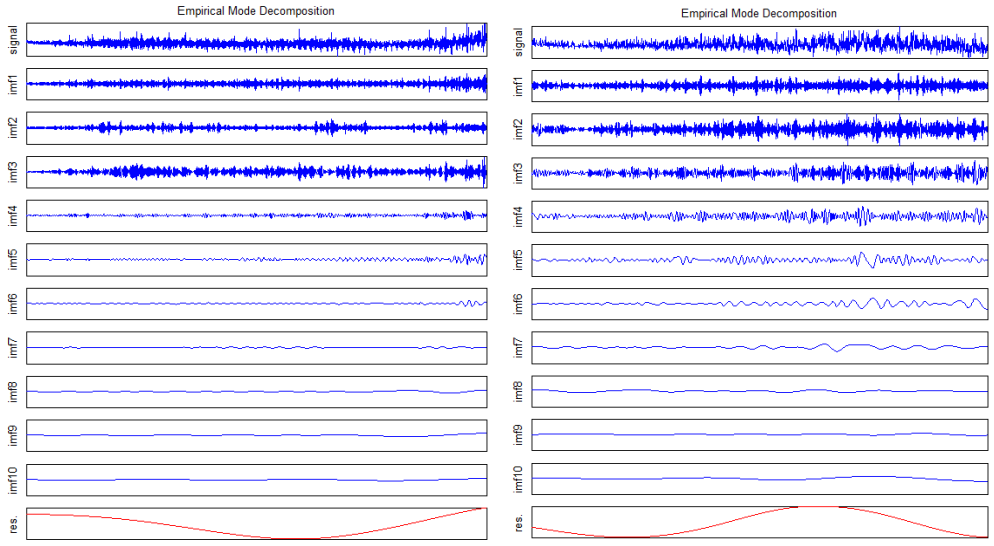

(a) (b)

Figure 20. EMD results of the torque of front drum with traction speed of 1.5 m/min: (a) experiment, (b) simulation

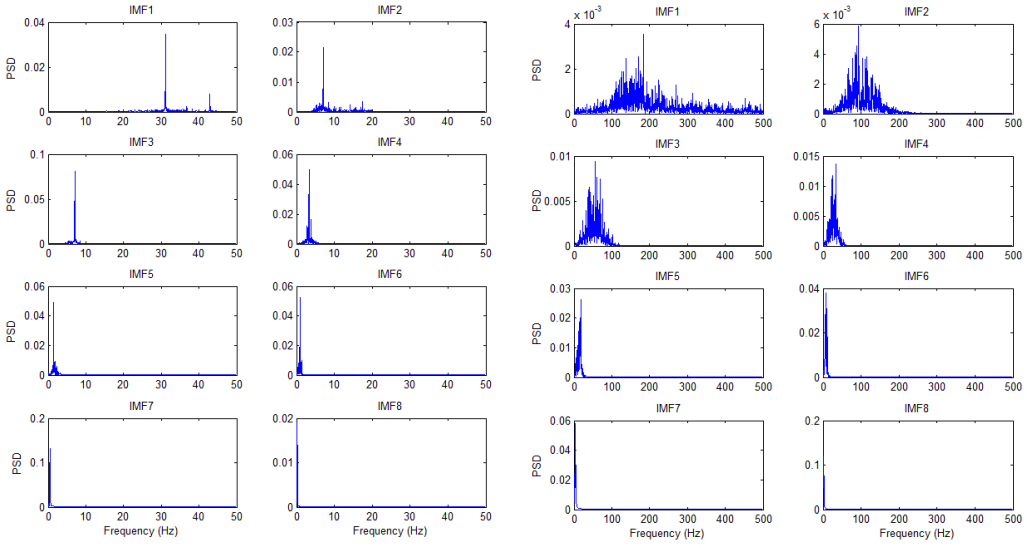

(a) (b)

Figure 21. Results of PSD analysis of the IMF components of front drum torque with traction speed of 1.5 m/min: (a) experiment, (b) simulation

Table 5. Results of analysis of front drum torque in frequency domain under different cutting conditions in experiments and simulations

Traction speed			IMF8	IMF7	IMF6	IMF5	IMF4	IMF3	IMF2	IMF1
1.5 m/min	Exp	Fre	0.2197	0.4639	0.952	1.416	3.296	7.08	7.08	31.05
		Amp	0.0139	0.1314	0.0525	0.0489	0.05	0.081	0.022	0.0345
	Sim	Fre	0.9766	3.174	7.324	18.8	34.42	56.4	93.51	183.1
		Amp	0.1097	0.0579	0.0378	0.0261	0.0137	0.0094	0.0058	0.0036
3 m/min	Exp	Fre	0.4639	0.9399	1.416	1.416	3.296	7.043	8.47	31.08
		Amp	0.0214	0.0248	0.0824	0.07	0.0241	0.0202	0.02	0.0025
	Sim	Fre	0.9766	4.883	8.789	19.29	24.66	65.92	93.75	138.9
		Amp	0.0831	0.0941	0.0273	0.0355	0.016	0.0121	0.0052	0.002
5 m/min	Exp	Fre	0.4761	0.9399	1.416	2.82	4.236	5.65	17.48	31.05
		Amp	0.0488	0.0313	0.0902	0.054	0.0332	0.019	0.0018	0.0123
	Sim	Fre	1.953	4.639	6.836	20.51	27.59	50.78	107.7	212.2
		Amp	0.0795	0.0827	0.0482	0.0369	0.0164	0.011	0.0058	0.0024

where Exp, Sim, Fre and Amp represent experiment, simulation, frequency and amplitude, respectively.

5. Conclusions

In this paper, a series of full-scale shearer cutting tests were conducted with different traction speeds. The pick forces and drum torque were monitored. Meanwhile, the shearer drum cutting models were built using PFC3D software. The cutting process were simulated under different cutting conditions and compared to the results obtained from experiments. The main conclusions are:

(1) The mean value and standard deviation of shearer drum torque (front or back) increase linearly with the increase of traction speed with high correlation coefficient. A reasonable agreement and significant correlations were found between experiment and simulation in terms of drum torque.

(2) The torque fluctuation coefficient decreases with the increase of traction speed. Although the standard deviation increases with the increase of traction speed, the torque fluctuates more stable in the condition of high traction speed. Besides, the torque fluctuation coefficients of back drum are larger than those of front drum. The fluctuation characteristic of drum torque was reproduced well in simulation comparing with experimental results.

(3) The energy consumption increased with the increase of traction speed in experiments, which was reproduced well in numerical simulation.

(4) The base frequency of drum torque is approximately 0.4667. The vibration of the torque consists of multiple frequencies below 50 Hz, and the drum torque is reproduced well by the PFC3D model in terms of characteristic frequency.

Therefore, the shearer drum cutting model built by PFC3D is reasonable and reliable in modeling the drum cutting process in different cutting conditions. Owing to the difficulty in conducting drum cutting tests in laboratory, the numerical simulation method for the prediction of drum forces can be adopted in selection and design shearers. Besides, considering the established empirical equations used in designing shearer drum now, the results of numerical simulation can be used for verifying the empirical results. Moreover, as the cutting process in PFC3D is recorded visualized and every particle can be traced, it's convenient to evaluate the loading efficiency of the drum in different cutting conditions. In the future work, the effects of kinematic parameters (i.e. traction speed and rotation speed of the drum) and structure parameters (i.e. pick arrangement,

number and dip angle of spiral vanes) of the drum on the cutting and loading efficiency will be investigated using this cutting model.

Acknowledgments: This research was supported by the National Basic Research Program of China (2014CB046301), the National Natural Science Foundation of China (U1510116, U1610251, U1610109), the Key Program of Shanxi Coal Basic (MJ2014-05), the Science and Technology Project of Jiangsu Province (BK20140051), a Project Funded by the Priority Academic Program Development of Jiangsu Higher Education Institutions (PAPD), National Research Foundation, South Africa (IFR160118156967 and RDYR160404161474), Yingcai project of CUMT (YC2017001). We are indebted to Zhangjiakou Coal Mine Machinery Co., Ltd. and Liaoning Technical University for the guidance and assistance provided.

.

References

1. Li Z.; Peng Z. *Nonlinear dynamic response of a multi-degree of freedom gear system dynamic model coupled with tooth surface characters: a case study on coal cutters*. Nonlinear Dynamics, 2016, 84, 271 – 286.

2. E.3.; B.3.; B.B. *The fracture theory of coal cut by shearer*, China Coal Industry Publishing House: Beijing, China, 1965; pp. 73-75.

3. Liu C.S.; Yu X.W.; Ren C.Y. *Drum shearer working organs*. Harbin engineering university press: Harbin, 2010; pp. 49-52.

4. Hekimoglu O.Z. The radial line concept for cutting head pick lacing arrangements. *International journal of rock mechanics and mining sciences & geomechanics abstracts. Pergamon*. 1995, 32(4), 301-311.

5. Khair A.W. Design and fabrication of a rotary coal cutting simulator. Proceedings of the Coal Mine Dust Conference, 1984.

6. Khair A.W.; Devilder W.M. Correlation of Fragment Size Distribution and Fracture Surface in Coal Cutting Under Various Conditions. Proceedings of the International Symposium on Respirable Dust in the Mineral Industries, the Pennsylvania State University, University Park, PA, 1986.

7. Achanti V.B. Parametric study of dust generation with rock ridge breakage analysis using a simulated continuous miner. PhD, West Virginia University, America, 1998.

8. Addala S. Relationship between cutting parameters and bit geometry in rotary cutting. PhD, West Virginia University, America, 2000.

9. Qayyum R.A. Effects of bit geometry in multiple bit-rock interaction. PhD, West Virginia University, America, 2003.

10. Liu S.Y.; Du C.L.; Cui X.X. Cutting experiment of the picks with different conicity and carbide tip diameters. *J China Coal Soc*. 2009, 34(9), 1276-1280.

11. Camargo H.E.; Gwaltney G.; Alcorn L.A. Development of an instrumented longwall bit to measure coal cutting forces for use in developing noise controls. *Mining Engineering*. 2015, 67(5), 57-62.

12. Eyyuboglu E.M.; Bolukbasi N.; Effects of circumferential pick spacing on boom type roadheader cutting head performance. *Tunn Undergr Sp Tech*. 2005, 20(5), 418-425.

13. Hekimoglu O.Z.; Ozdemir L. Effect of angle of wrap on cutting performance of drum shearers and continuous miners. *Mining Technology*. 2004, 113(2), 118-122.

14. Yu B. Numerical simulation of continuous miner rock cutting process. PhD, West Virginia University, America, 2005.

15. Mishra B. Analysis of cutting parameters and heat generation on bits of a continuous miner-using numerical and experimental approach. ProQuest. 2007.

16. Su O.; Akcin N.A. Numerical simulation of rock cutting using the discrete element method. *Int J Rock Mech Min.* 2011, 48(3), 434-442.

17. Rojek J.; Oñate E.; Labra C.; et al. Discrete element simulation of rock cutting. *Int J Rock Mech Min. 2*011, 48(6), 996-1010.

18. Van Wyk G.; Els D.N.J; Akdogan G.; et al. Discrete element simulation of tribological interactions in rock cutting. *Int J Rock Mech Min*. 2014, 65, 8-19.

19. ASTM. (1995). Standard test method for unconfined compressive strength of intact rock core specimens. American Society for Testing and Materials, D2938.

20. ASTM. (1995). Standard test method for splitting tensile strength of intact rock core specimens. American Society for Testing and Materials, D3967.

21. Liu Y.J.; Li Y.X. Revisit of the equivalence of the displacement discontinuity method and boundary element method for solving crack problems, *Engineering Analysis with Boundary Elements*. 2014, 47, 64-67.

22. Potyondy D.O. The bonded-particle model as a tool for rock mechanics research and application: current trends and future directions. *Geosystem Engineering*. 2015, 18(1), 1-28.

23. Shi J.Y.; Shen B.T.; Stephansson O.; Rinne M. A three-dimensional crack growth simulator with displacement discontinuity method, *Engineering Analysis with Boundary Elements*. 2014, 48, 73-86.

24. Krolczyk G.; Gajek M.; Legutko S. Effect of the cutting parameters impact on tool life in duplex stainless steel turning process. *Tehnički Vjesnik-Technical Gazette*. 2013, 20(4), 587-592.

25. Yue X.; Tao C.D. Optimization of parameters for design of spiral cutting drum of shearer. *J China Coal Soc*. 1996, 21(5), 542-546.

26. Yang M.Q.; Li S.G.; Wang C.B. Application of the torque fluctuation coefficient method to the monitoring of bit performance. *Natural Gas Industry*. 2013, 33(6), 76-79.

27. Balci C.; Demircin M.A.; Copur H.; et al. Estimation of optimum specific energy based on rock properties for assessment of roadheader performance. *JS Afr Inst Min Metall*. 2004, 104(11), 633-642.

28. Wu R.; Xu J.H.; Li C.; Wang Z.L.; Qin S. Stress distribution of mine roof with the boundary element method, *Engineering Analysis with Boundary Elements*, 2016, 50, 39-46.

29. Rilling G.; Flandrin P.; Goncalves P. On empirical mode decomposition and its algorithms. IEEE-EURASIP workshop on nonlinear signal and image processing. IEEER, 2003, 3, 8-11.

30. Li L. Analysis of mechanical signal and application. Huazhong University of Science and Technology Press, Wuhan, 2007.

31. Guo X.H.; Xu X.H; Zhao S.Q. Noising reduction algorithm based on empirical mode decomposition (EMD) and applications in calculating trajectories of spacecraft. *Journal of Astronautics*, 2008, 4, 1272-1307.

32. Xuefeng Li, Shibo Wang, Shangqing Hao, Zhixiong Li, "Numerical Simulation of Rock Breakage Modes under Confining Pressures in the Rock Cutting Process: an Experimental Investigation, IEEE Access, Vol.4, pp.5710-5720, 2016.

33. Xiangjun Jin, Jie Shao, Xin Zhang, Wenwei An, "Modeling of nonlinear system based on deep learning framework", Nonlinear Dynamics, Springer, Vol.84, No. 3, pp.1327-1340, 2016